Received: 3 September 2021 | Revised: 21 October 2022 | Accepted: 28 October 2022 | Published on: 9 November 2022

DOI: 10.1002/joc.7910

RESEARCH ARTICLE

International Journal of Climatology RMetS

Individual local human thermal climates in the Hungarian lowland: Estimations by a simple clothing resistance-operative temperature model

Ferenc Ács[1] | **Erzsébet Kristóf**[1] | **Annamária Zsákai**[2]

[1]Department of Meteorology, Faculty of Science, Institute of Geography and Earth Sciences, Eötvös Loránd University, Budapest, Hungary

[2]Department of Human Anthropology, Faculty of Science, Eötvös Loránd University, Budapest, Hungary

Correspondence
Ferenc Ács, Department of Meteorology, Faculty of Science, Institute of Geography and Earth Sciences, Eötvös Loránd University, 1117 Budapest, Hungary.
Email: acs@caesar.elte.hu

Abstract

Human thermal climate in the Hungarian lowland is investigated by using a clothing resistance-operative temperature model performing individual, local, and long-term concurrent observations of weather and human thermal perception. Human thermal load is characterized in terms of clothing resistance r_{cl} and operative temperature T_o. The model is also used as a tool to analyse the relationship between r_{cl} and the structural parameters of the body (relative fat mass index (fatBMI) and relative muscle mass index (muscleBMI)). This analysis works with data collected on more than 1,000 occasions of weather and thermal perception observation and uses body structure data of more than 3,000 adults and children. By analysing the data, the following human thermal climate characteristics have been established. (a) T_o of about 80°C can be considered as the upper limit of heat stress in the Hungarian lowland, similarly, T_o of about −35 to −37°C can be taken as the lower limit of cold stress. (b) Interpersonal thermal load variations increase with increasing of cold stress; these variations are the smallest within the "thermoneutral" zone. (c) In cold stress situations, there is a significant sexual dimorphism in the relationship between r_{cl} and fatBMI. (d) In night time period of the day, T_o can vary between 25°C and the lower limit of cold stress. In this range of T_o, thermal perception types "neutral," "cool," "cold," and "very cold" occurred. Based on the results, it can be seen that interpersonal thermal load variations cannot be neglected in extreme cold weather conditions, and that interpersonal variations of fatBMI index are determinant in the formation of individual clothing resistance.

KEYWORDS

clothing resistance, cold stress, Hungarian lowland, individuals, interpersonal variations, operative temperature, relative fat mass index, weather

1 | INTRODUCTION

Today, energy balance-based models are already the most common (Potchter *et al*., 2018) in human thermal load studies. According to Potchter *et al*. (2018), among energy balance-based indices, those most frequently used are PMV (Predicted Mean Vote), PET (Physiologically Equivalent Temperature), and UTCI (Universal Thermal Climate Index). The PMV model is the simplest, it is a one-segment, one-node model (Enescu, 2019) constructed by Fanger (1970) assuming quasi-steady-state conditions. The model does not contain any thermoregulation process description. The model was developed for indoor conditions. It assumes that people are sitting and that the clothes they are wearing completely cover their bodies. The thermal load–thermal sensation relationship is experimentally established. In Fanger's (1970, 1973) experiments, thermal perception observation is made by a large number of people (a total of 1,300 people participated in the observations) using a seven-point scale from "cold" (PMV = −3) to "hot" (PMV = +3), which represents the expected average thermal sensation vote. People sat in standard clothing in microclimate-controlled rooms. The UTCI index model, on the other hand, is one of the most complex models. It appeared about 40 years later than the Fanger model (Fiala *et al*., 2011; Havenith *et al*., 2012) and since it is so complex there is also a simpler statistical-deterministic version (Bröde *et al*., 2012) of it. According to Enescu (2019), the UTCI index model contains 12 segments and 187 nodes. It is designed for simulating transient, non-steady state, both indoor and outdoor environmental conditions, including extreme weather conditions, thus it is also suitable for simulating dynamic thermal sensation, that is, the change of thermal perception over time. In the Fiala model (Fiala, 1998), in establishing the thermal load–thermal perception relationship many older experimental results (Nevins *et al*., 1966; McNall *et al*., 1967; Rohles, 1970) were used beside results obtained by observations made by 10 subjects (5 male and 5 female) using the seven-point scale that Fanger also used. As in Fanger's experiments, the observation of thermal perception took place indoors, in microclimate-controlled rooms, in which hundreds of people participated. The PET index model is between the PMV and UTCI index models in terms of complexity. In the PET index model, the concept of Gagge *et al*. (1971) is applied, which is based on the use of "standard human" and "standard environment." Like all models, it went through different phases of development. The main phases of its development can be found in the works of Höppe (1984, 1993, 1999), Mayer and Höppe (1987), Matzarakis and Mayer (1996, 1997), and Matzarakis *et al*. (1999, 2007). PET index model can be used for several purposes: to investigate topics such as (a) human thermal comfort (e.g., Milošević *et al*., 2016), (b) indoor/outdoor thermal climates (e.g., Staiger *et al*., 2019), (c) urban microclimates (e.g., Pecelj *et al*., 2021), and (d) rural/urban thermal environments (e.g., Unger *et al*., 2020) and climate classification (Gulyás and Matzarakis, 2009). Today, it is used as a software package (Matzarakis *et al*., 2007); this is one of the reasons why it is the most widely used human biometeorological index in the world. In the PET index model, the thermal perception types are based on the PMV model thermal perception types (Matzarakis and Mayer, 1996), which means that they were determined based on the comparison of the results of the PET model and the PMV model. According to Enescu (2019), PET index model possesses one segment and two nodes. In the Carpathian Basin region, PET and UTCI are used most frequently. These two indices are constructed for investigating human thermal comfort; therefore, they also contain subroutines for describing human thermoregulation processes.

It is the concept of a "standard human," that has become dominant in the science of human biometeorological modelling. This same model of the "standard human" is also used in the case of empirical indices, which are not based on the energy balance of the human body covered by clothing. For instance, in Mohan *et al*.'s (2014) study, the Heat Index refers to a person, who is 170 cm tall, weighs 67 kg, walks in the shade at a speed of 1.5 $m \cdot s^{-1}$ in a light breeze of 2.7 $m \cdot s^{-1}$, wearing long pants and a short-sleeved shirt. It should be noted that the characteristics of the "standard human" vary from index to index. For instance, in PET, the "standard human" is a 35-year-old man, who has a body weight of 75 kg, a body length of 180 cm, he is standing (metabolic heat flux density is about 80 $W \cdot m^{-2}$) in a room, and possesses a typical indoor setting of 0.9 clo (Höppe, 1999). UTCI uses an average person (e.g., Blazejczyk *et al*., 2010, 2013) with a body weight of 73.5 kg, a body fat content of 14% and a Dubois-area of 1.86 m^2. Sex is not specified. This person is walking in outdoor conditions at a speed of 1.1 $m \cdot s^{-1}$. His/her clothing is estimated according to a clothing model (Havenith *et al*., 2012), which represents the clothing patterns of European and North American urban populations. The clothing model is integrated into the UTCI-Fiala model (Fiala *et al*., 2011). It can be seen that not only human characteristics change, but also clothing. It should be mentioned that the variability of clothing is much greater, as can be seen from the previous cases, because its variability is also affected by individual, psychological and cultural factors. What is more, this variability can also be traced in its historical development (Gilligan, 2010). It is obvious that the representation of clothing in biometeorological models is a very

important, but difficult task because of its highly variable insulation value. The role of clothing together with activity and climate on human thermal comfort is a well-known subject in its physical foundation. Such analyses can be found, for instance, in the work of Fanger (1973), Blazejczyk and Krawczyk (1994), Ogulata (2007), or Innova Air Tech Instruments (2002).

In all three models, regardless of the complexity, the thermal insulation value of the clothing is an input parameter. Skin temperature, core temperature, or the clothing's surface temperature are the variables to be calculated. For this, we usually say that the model works in "forward mode." However, there are also models in which the state variables are known and the objective is to estimate the thermal insulation of the clothing, in such cases, we usually say that the model works in "backward mode." Based on the terminology and the model types introduced, we can easily define our model type (Ács *et al.*, 2021b): it is a Fanger model (one-segment, one-node) used in "backward mode" (clothing resistance is not an input, but rather an output variable). It calculates the thermal insulation value of virtual clothing (r_{cl}), which achieves the thermal equilibrium between the human body and the environment. This methodology cannot be used in warm climates, because in these cases the r_{cl} would be negative, which is impossible given the definition of r_{cl}. In warm climates, the methodology does not meet the energy balance because it does not simulate the process of sweating under clothing. However, we preferred this model type because of its extreme simplicity, which is a central requirement in models for climate classification purposes.

It should be mentioned that studies on individualization already exist. Zhou *et al.* (2013) modified human thermoregulation of the UTCI-Fiala model and embedded Chinese adults' anthropometric characteristics. The modification significantly improved the prediction of mean and local skin temperatures. Other attempts have been made by Ács *et al.* (2021a, 2021b). In these studies, a person walking at a speed of 1.1 $m{\cdot}s^{-1}$ is analysed. The model used is much simpler than the UTCI-Fiala model, for instance, thermoregulation processes are not taken into consideration. The main conclusion is that human thermal load depends significantly on human somatotype. Ács *et al.* (2021b) also demonstrated that large somatotype differences are associated with large differences in metabolic heat production (M). To the best of our knowledge, interpersonal human thermal climate deviations have not yet been thoroughly investigated. It is also becoming more and more obvious that the thermal load and thermal sensation experienced by a human varies during the course of human life.

Based on the above, the aims of this study are as follows: (a) to present a simple human thermal load and sensation model, (b) to perform extensive tests on model sensitivity to the changes of human and atmospheric variables, and (c) to gain knowledge of individual, local human thermal climate characteristics in the Hungarian lowland region on the basis of weather observations.

2 | METHODS

Concerning the methodology, the project is built using three procedures and three human body composition parameters. The procedures include a scheme for characterizing environmental human thermal load, human thermal sensation observations, and a data management method to establish a statistical link between thermal load and thermal sensation data. Thermal load is characterized in terms of clothing resistance and operative temperature. As far as human body composition parameters are concerned, body mass index (BMI), relative fat mass index (fatBMI), and relative muscle mass index (muscleBMI) are introduced and used.

2.1 | Human body composition parameters

The BMI, fatBMI, and muscleBMI indices are defined as follows,

$$BMI = \frac{M_{bo}}{\left(\frac{L_{bo}}{100}\right)^2}, \tag{1}$$

$$fatBMI = \frac{fatM_{bo}}{\left(\frac{L_{bo}}{100}\right)^2}, \tag{2}$$

$$muscleBMI = \frac{muscleM_{bo}}{\left(\frac{L_{bo}}{100}\right)^2}, \tag{3}$$

where M_{bo} is the total body mass (kg), $fatM_{bo}$ is the total body fat mass (kg), $muscleM_{bo}$ is the total body skeletal muscle mass (kg) and L_{bo} is the body length (cm). Note that all three body composition indices are expressed in $kg{\cdot}m^{-2}$ dimensions. The required data (body, fat, and skeletal muscle masses) are determined by a body composition analyser (bioelectrical impedance analyser): InBody 720. This multifrequency bioelectrical impedance analyser estimates impedance (resistance, reactance) on the basis of total tissue response to the electric current flowing at different rates through the body. Total body water mass, fat-free and fat masses as well as skeletal muscle mass are estimated by the equipment considering the impedance measures, the body dimensions (body

weight and length), and the biological indicators of body composition (sex, age) (Finn *et al.*, 2015).

2.2 | The clothing resistance-operative temperature model

The clothing resistance-operative temperature model is a Fanger model used in "backward mode," consequently clothing resistance is an output variable. It is expressed on the basis of clothed human body energy balance considerations (Ács *et al.*, 2021a) as

$$r_{cl}=\rho\cdot c_p\cdot\frac{T_S-T_o}{M-\lambda E_{sd}-\lambda E_r-W}-r_{Hr}, \tag{4}$$

where ρ is air density (kg·m^{-3}), c_p is specific heat at constant pressure (J·kg^{-1}·°C^{-1}), r_{Hr} is the combined resistance for expressing the thermal radiative (r_{R}) and convective (r_{Ha}) heat exchanges (s·m^{-1}), T_{S} is skin temperature (°C), T_{o} is operative temperature (°C), M is metabolic heat flux density (W·m^{-2}), λE_{sd} is the latent heat flux density of dry skin (W·m^{-2}), λE_r is respiratory latent heat flux density (W·m^{-2}), and W is mechanical work flux density (W·m^{-2}). r_{cl} refers to a walking human in outdoor conditions whose speed is 1.1 m·s^{-1} (4 km·h^{-1}) and skin temperature is 34°C. We can see that the dimension of r_{cl} is (s·m^{-1}) (inverse of m^3·m^{-2}·s^{-1}). Dimension of $r_{\mathrm{cl}}/(\rho\cdot c_p)$ is (m^2·°C/W), which is also a resistance dimension, so r_{cl} (s·m^{-1}) = 1,204.8·r_{cl} (m^2·°C/W). Since clothing resistance of 1 (clo) is 0.155 (m^2·°C/W), so 1 (clo) is 1,204.8·0.155 = 186.74 (s·m^{-1}). The clothing thermal resistance cannot be negative because in these cases the energy balance is not met since the process of sweating under clothing is not simulated. When r_{cl} is close to 0, thermal load is very small. Environmental resistances r_{Hr}, r_{R}, and r_{Ha} are interconnected as

$$\frac{1}{r_{Hr}}=\frac{1}{r_{Ha}}+\frac{1}{r_R}, \tag{5}$$

where

$$r_{Ha}\left[sm^{-1}\right]=7.4\cdot 41\cdot\sqrt{\frac{D}{U_{1.5}}}, \tag{6}$$

$$\frac{1}{r_R}=\frac{4\epsilon_{cl}\sigma T_a^3}{\rho c_p}, \tag{7}$$

where D (m) is the diameter of the cylindrical body with which the human body is approximated (Campbell and Norman, 1998), $U_{1.5}$ is air speed relative to the human body at 1.5 m, $\varepsilon_{\mathrm{cl}}$ is the emissivity of clothing or skin (in this study, $\varepsilon_{\mathrm{cl}}$ = 1), σ is the Stefan-Boltzmann constant, and T_{a} is air temperature (°C). $U_{1.5}$ is calculated using wind speed data at a height of 10 m and using a logarithmic wind profile supposing neutral thermal stability. The scheme does not consider the effect of the direction of a walking human compared to the direction of wind speed. We assume that this additional information is not important in the majority of cases (Ács *et al.*, 2019).

Operative temperature represents atmospheric thermal load, it can be considered as independent from human factors. It can be expressed as

$$T_o=T_a+\frac{R_{ni}}{\rho\cdot c_p}\cdot r_{Hr}, \tag{8}$$

where R_{ni} is isothermal net radiation. R_{ni} is estimated as simply as possible as

$$R_{ni}=S\cdot(1-\alpha_{cl})+\epsilon_a\sigma T_a^4-\epsilon_{cl}\sigma T_a^4, \tag{9}$$

where S is the global radiation, α_{cl} is the albedo of clothing, ϵ_a is the atmospheric emissivity, and ϵ_{cl} is the emissivity of clothing or skin. In this scheme α_{cl} = 0.25–0.27. Global radiation is estimated via relative sunshine duration *rsd* according to Mihailović and Ács (1985).

The human does not sweat and walks at a speed of 1.1 m·s^{-1}. The human's total metabolic heat flux density can be expressed as

$$M=M_b+M_w, \tag{10}$$

where M_b is the basal metabolic rate (W) and M_w is the metabolic rate (W) referring to walking. M_b is parameterized according to Mifflin *et al.* (1990) separately for men and women

$$M_b^{male}\left[kcal\cdot day^{-1}\right]=9.99\cdot M_{bo}+6.25\cdot L_{bo}-4.92\cdot age+5, \tag{11}$$

$$M_b^{female}\left[kcal\cdot day^{-1}\right]=9.99\cdot M_{bo}+6.25\cdot L_{bo}-4.92\cdot age-161. \tag{12}$$

where M_{bo} is body mass (kg), L_{bo} is body length (cm), and *age* is expressed in years. The human body surface A (m^2) has to be estimated to express M_{b} in W·m^{-2}, and for this we use the well-known Dubois and Dubois (1915) formula,

$$A=0.2\cdot M_{bo}^{0.425}\cdot\left(\frac{L_{bo}}{100}\right)^{0.725}. \tag{13}$$

M_w is parameterised according to Weyand *et al.* (2010) as follows,

$$M_w = 1.1 \cdot \frac{3.80 \cdot M_{bo} \cdot \left(\frac{L_{bo}}{100}\right)^{-0.95}}{A}. \quad (14)$$

The coefficient 1.1 is added because of the chosen walking speed. The $\lambda E_{sd} + \lambda E_r$ sum in Equation (4) can be expressed as a function of M according to Campbell and Norman (1998) as

$$\lambda E_r + \lambda E_{sd} = \frac{e_S(T_S) - e_a}{p_a} \cdot [1.83 \cdot M + 237.6]. \quad (15)$$

where e_S (T_S) is the saturation vapour pressure (hPa) at temperature T_S, e_a is the actual vapour pressure (hPa), and p_a is the atmospheric pressure (hPa) at ground level.

W is parameterized according to Auliciems and Kalma (1979) as

$$W = 0.25 \cdot (M - M_b). \quad (16)$$

2.3 | Estimation of thermal sensation

Human thermal sensation observations are made by two persons, one is male and the other female. The observation times are randomly distributed. There are observations at all times of the day (morning, evening, noon, night, and afternoon), and the number of observations is 450–600 for both persons. Their human state variables are presented in Table 1. Even though the human thermal sensation scale is continuous, it is always discrete scales that are used (Enescu, 2019) to register thermal sensation types. The most frequently used scale is a 7-grade scale, which is as follows: "very warm," "warm," "slightly warm," "neutral," "cool," "cold," and "very cold." As it can be seen, we have chosen a terminology that is more realistic; for instance "very warm" is warmer than "warm" but colder than "hot"; or "slightly cool" is not used to be able to distinguish "neutral" from "cool" as clearly as possible. The observations are performed according to the rules as follows:

1. always go outdoors with a "neutral" thermal perception
2. always strive to perform the observation at the same location
3. the microclimate of the observation site should reflect standard weather conditions (weather observed) as much as possible,
4. do not stay in the shade when the sun is shining
5. do not grasp or touch anything
6. we have to leave as much body surface free of clothing as possible
7. do not stand barefoot on the ground and do not wear hat, gloves or a scarf while walking or standing
8. stay outside for at least 5 min, and
9. use a 7-grade scale for indicating your thermal sensation.

Both persons are native to the region of the Hungarian lowland, where the climate can be characterized either as *Cfb* (*C*—warm temperate, *f*—no seasonality in the annual course of precipitation, *b*—warm summer) according to Köppen (1936), or as "cool and dry with extreme variations of temperature" according to Feddema (2005). During thermal sensing (usually lasting 5 min), sweating or shivering did not occur, of course, the observers were not aware of their vasodilation or vasoconstriction processes, not to mention other hidden thermoregulatory processes.

2.4 | Management of thermal sensation and thermal load data

Weather and thermal sensation data are collected concurrently. Thermal load is estimated from weather and human data by using our model. Both observers used their own data. First, the consistency between thermal load and thermal sensation data is checked. All those observations are removed where positive clothing resistance values are associated with the thermal sensation types "slightly warm" or "warm."

3 | LOCATIONS OF OBSERVATIONS

The locations of the towns where weather, thermal sensation and human anthropometric data were collected are presented in Figure 1. Martonvásár is about 30 km southwest of Budapest. The location in Budapest, where the individual observations took place, is in District 14, in the suburbs. The location, where the people were interviewed, was the square next to the ELTE building (District 11). The towns are located in the lowland regions of Hungary. Their climate is *Cfb* according to Köppen (1936) or "cool and dry with extreme variations of temperature" according to Feddema (2005).

4 | DATA

There are two types of data: weather data and human data. The main features of data are discussed below.

TABLE 1 Human state variables and metabolic heat flux densities of two persons (person 1: a male and person 2: a female)

Persons	Sex	Age (years)	Body mass (kg)	Body length (cm)	Basal metabolic heat flux density ($W \cdot m^{-2}$)	Walking energy flux density ($W \cdot m^{-2}$)	Total energy flux density ($W \cdot m^{-2}$)
Person 1	Male	64	89.0	190.0	40.8	94.5	135.3
Person 2	Female	34	64.5	160.5	38.6	103.9	142.5

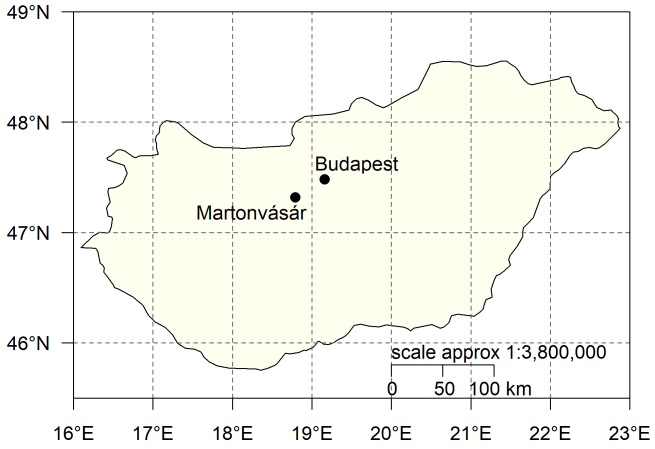

FIGURE 1 The locations of the towns where the collection of weather data is carried out and the thermal sensation observations are performed [Colour figure can be viewed at wileyonlinelibrary.com]

4.1 | Weather data collected by individuals

From the weather data, air temperature, relative humidity of air, average wind speed, gust, surface air pressure, cloud cover and relative sunshine duration are used. All data, except for the latter two, are taken from automatic stations belonging to the Hungarian Meteorological Service (HMS) or to the private company "Időkép" (https://www.idokep.hu/). The beeline distance between the stations and the observers' locations was shorter than 3 km. Cloud cover and relative sunshine duration data are provided by the observers. Cloud cover is estimated visually in tenths. Relative sunshine duration refers to the observer's body because the human body's thermal load is to be estimated.

The observations of person 1 were in the period April 1, 2020 to June 29, 2021. In this period, the weather was very changeable. Surface air pressure ranged from 994 to 1,036 hPa, but there were only three observations when the air pressure was less than 1,000 hPa. There were both nighttime (global radiation is equal to 0) and daytime (global radiation is larger than 0) observations. About 40% of the observations were made in the nighttime period. Then air temperature ranged between −11 and 28°C, the wind speed was low in the vast majority of cases, but there were also windy cases, when the average wind speed was very high (between 4 and 7 $m \cdot s^{-1}$). Relative air humidity varied between 40 and 100%. In the daytime period, global radiation varied between 10 and 850 $W \cdot m^{-2}$, while air temperature between −9 and 32°C. Wind was moderate (2–3 $m \cdot s^{-1}$) in most cases, but there were also lower (under 1 $m \cdot s^{-1}$) and higher (average wind speed about 6–7 $m \cdot s^{-1}$, gusts above 10 $m \cdot s^{-1}$) wind speed values. Relative humidity ranged between 20 and 100%.

Person 1 also collected weather data to investigate clothing resistance–body composition parameter relationships. Weather data for one winter (February 28, 2018) case are used, these are presented in Table 2.

In Hungarian lowland, this cold weather counts as extreme.

The observation period of person 2 was between April 1, 2020 and August 14, 2021. About two-thirds of observations refer to anticyclonic weather situations. There was no precipitation during the observations. Surface air pressure varied between 993 and 1,038 hPa. During the nighttime period observations (about 35% of observations), air temperature varied between −10 and 23°C, relative humidity between 40 and 100%, and average wind speed between 0.1 and 6.7 $m \cdot s^{-1}$. In the daytime period, these changes were somewhat greater. Air temperature ranged between −9 and 34°C, relative humidity between 15 and 100%, and average wind speed between 0.1 and 7.8 $m \cdot s^{-1}$.

4.2 | Weather data collected during interview periods

The phenomenon of interpersonal thermal perception variability is also tested by interviewing people. To estimate thermal load during the interview period, weather data also needs to be collected. Field data collection was performed on February 18, 2020 between 11 a.m. and 4 p.m. and on February 19, 2020 between 10 a.m. and 2 p.m. Weather data are provided by the meteorological station installed at the research facility BpART (Budapest platform for Aerosol Research and Training; http://salma.web.elte.hu/BpArt/). The BpART meteorological station is basically a station supporting aerosol research, but it also provides meteorological data supporting other

TABLE 2 Meteorological conditions in Martonvásár on February 28, 2018 at 7 a.m

Date	Meteorological conditions					
	Ta (°C)	rsd	N	va (m·s−1)	rh (%)	pa (hPa)
February 28, 2018	−10.0	0	1.0	3.0	85	1,018

Note: Symbols: T_a—Air temperature, rsd—Relative sunshine duration, N—Cloudiness, v_a—Average wind speed, rh—Relative humidity of air, p_a—Atmospheric pressure.

research goals (e.g., Salma *et al.*, 2020). Air temperature, relative humidity of air, wind speed, wind direction, and global radiation are measured generating their 1-min values. Cloudiness is estimated visually on site. Air temperature varied between 9 and 12°C, relative humidity between 40 and 70%, and average wind speed ranged from 1 to 7 $m \cdot s^{-1}$. Cloudiness was very variable, it varied from 0.3 to 1, but in most cases, it was between 0.7 and 1. Correspondingly, global radiation ranged from 50 to 550 $W \cdot m^{-2}$.

4.3 | Human data

There are three human data types: (a) anthropometric data characterizing the Hungarian population contained in a Hungarian human data set, (b) human state variables together with metabolic heat flux densities of persons 1 and 2, and (c) human state variables and thermal perception votes of the people participating in the interview. Anthropometric data needed for calculating body composition parameters (body mass index, relative fat mass index and relative muscle mass index) and metabolic heat flux densities are contained in the Hungarian human data set (Utczás *et al.*, 2015; Zsákai and Bodzsár, 2016; Fehér *et al.*, 2019) created at the Department of Biological Anthropology, Eötvös Loránd University, Budapest, Hungary. The human data set contains the data of more than 2,000 Hungarian children and more than 1,000 Hungarian adults. They participated in the cross-sectional surveys of the Department of Biological Anthropology in 2010. The participants of the surveys were always informed of the details of the project, and all provided written consent.

The human state variables and metabolic heat flux densities of persons 1 and 2, who performed longitudinal study, are presented in Table 1.

People participating in the interview reported on their human state variables (body mass, body length, sex, and age). No other demographic data were collected. In addition to these data, the clothing worn and the subjective thermal sensation vote (TSV) responding on the discrete 7-point thermal sensation scale (see point 9 in Section 2.3) were also registered. In total, 87 people are interviewed.

5 | RESULTS

Four result types are analysed for individuals and five result types for human groups. For individuals, the r_{cl}–T_o relationship, the thermal sensation–r_{cl} or thermal sensation–T_o relationship, the T_o–T_a relationship, and the r_{cl}–UTCI (Universal Thermal Climate Index), T_o–UTCI relationships are considered. For human groups, first, the interpersonal variations of BMI, M, and thermal perception are analysed; later on, the r_{cl}–fatBMI and the r_{cl}–muscleBMI relationships are discussed by performing sensitivity tests.

5.1 | Interpersonal variations of BMI, *M*, and thermal perception

In this study, thermal perception evaluations are made by persons 1 and 2. This is why their human characteristics are important and these are compared to the characteristics of other people in the Hungarian database. A scatter chart of total (basal plus walking) energy flux density as a function of BMI for all people in the Hungarian data set together with persons 1 (black circle) and 2 (black triangle) is presented in Figure 2.

Red circles represent males, while blue circles females. BMI values vary between 15 and 45 $kg \cdot m^{-2}$, but the vast majority of points are located between 17 and 35 $kg \cdot m^{-2}$. The BMI values of persons 1 and 2 are very close to 25 $kg \cdot m^{-2}$, which is the median of BMI values. For the median value of BMI, M varies between 135 and 148 $W \cdot m^{-2}$, that is, the interpersonal variability of M is roughly 10%. In all other cases, the interpersonal variability of M is less than 10%.

Regarding interpersonal thermal perception variations in the interview periods, the situation is as follows. The BMI values of 87 people varied between 17 and 37 $kg \cdot m^{-2}$, but the number of people with a BMI of around 25 $kg \cdot m^{-2}$ (between 22 and 27 $kg \cdot m^{-2}$) is just 34. The variability of T_o or UTCI is caused mainly by variations of global radiation, which is governed by changes of cloudiness. T_o varied between 35 and 6°C, while UTCI between 9.9 and 25.9°C. During these thermal loads, the following thermal perceptions were registered: 8 votes for

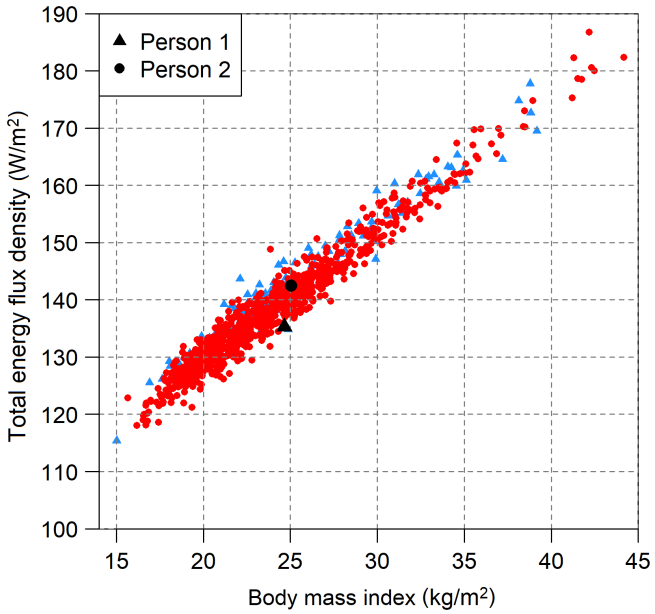

FIGURE 2 Scatter chart of total energy flux density used during walking as a function of body mass index for the Hungarian human data set. Blue: Males, red: Females [Colour figure can be viewed at wileyonlinelibrary.com]

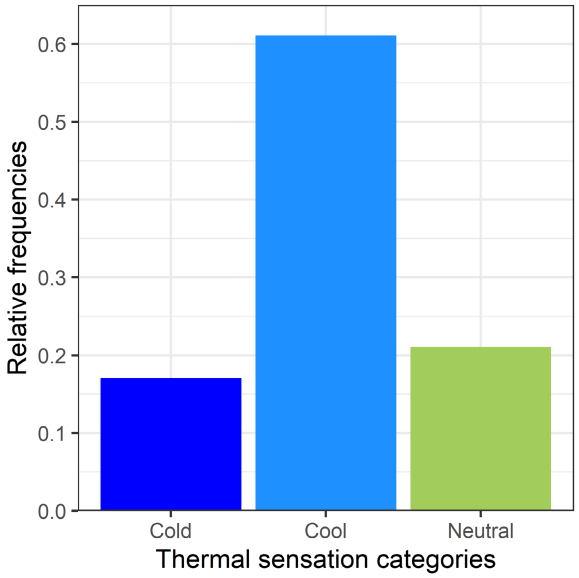

FIGURE 3 Relative frequency distribution of thermal sensation categories for 34 people [Colour figure can be viewed at wileyonlinelibrary.com]

"neutral," 19 votes for "cool," and 7 votes for "cold" thermal perception categories. The corresponding relative frequency distribution is presented in Figure 3. Note that these TSV variations are caused not only by personal but also by weather variations.

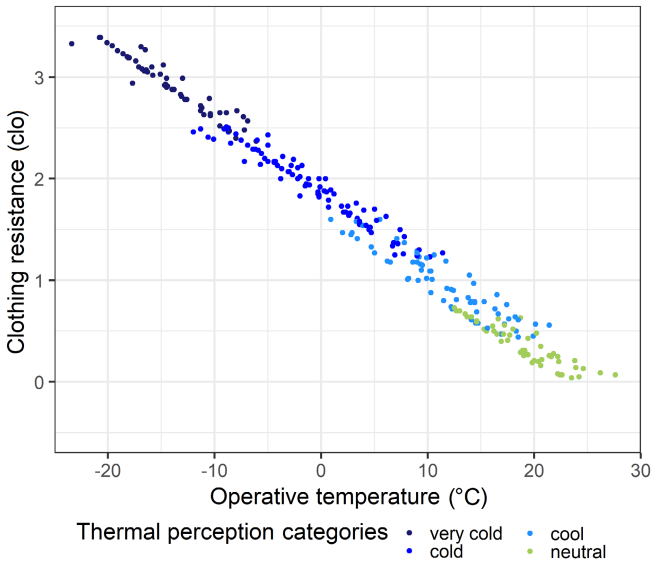

FIGURE 4 Scatter chart of clothing resistance of person 1 as a function of operative temperature at actual average wind speed (the average value of actual average wind speed is 1.31 $m \cdot s^{-1}$) [Colour figure can be viewed at wileyonlinelibrary.com]

As we see, the thermal perception category "cool" is the most frequent, the adjacent thermal categories are practically equally represented.

5.2 | Individual clothing resistance–operative temperature relationships

Operative temperature characterizes the weather's thermal load. Although it depends on human chest size through r_{Ha}, but since the dependence is weak, it can be viewed as human-independent parameter. Clothing resistance depends on both human and weather factors since, besides operative temperature, it also depends on metabolic heat flux density. Because of this, each r_{cl}–T_o relationship is individual and varies from person to person. The r_{cl}–T_o scatter chart for person 1 is presented in Figure 4.

We can also see that these points are coloured according to thermal perception categories, so the thermal load–thermal sensation relationship can also be observed. The most important human climatological information is as follows: (a) at the observation site, r_{cl} can vary between 3.5 and 0 clo, (b) the corresponding range of T_o is between −22 and 25°C, (c) T_o and r_{cl} values for neutral thermal sensation are around 25°C and 0 clo, respectively, and (d) the points referring to adjacent thermal sensation categories (e.g., cool/cold or cool/neutral) overlap each other, clearly showing that the thermal sensation scale is continuous and difficult to discretise. The

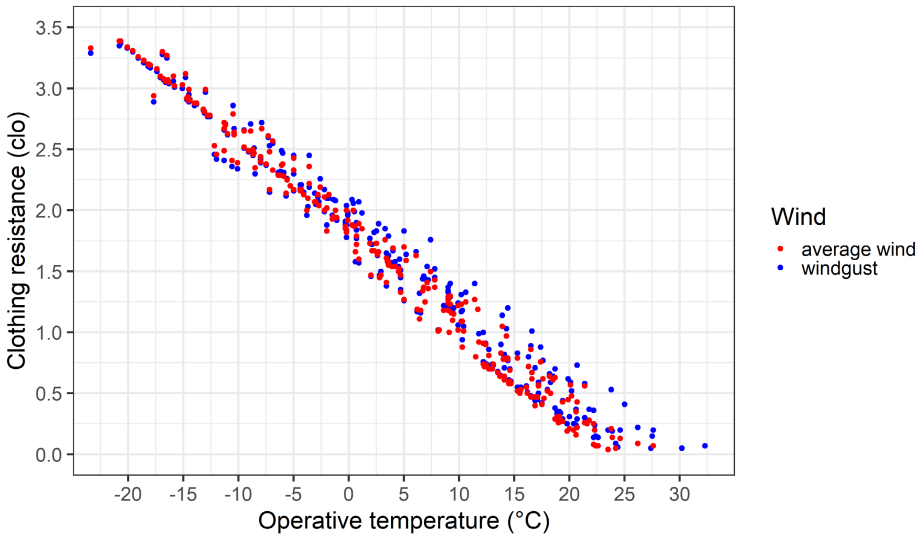

FIGURE 5 Scatter chart of clothing resistance of person 1 as a function of operative temperature at actual average wind speed (red) and gust (blue) (the average value of actual average wind speed and gust is 1.31 and 2.38 $m \cdot s^{-1}$, respectively) [Colour figure can be viewed at wileyonlinelibrary.com]

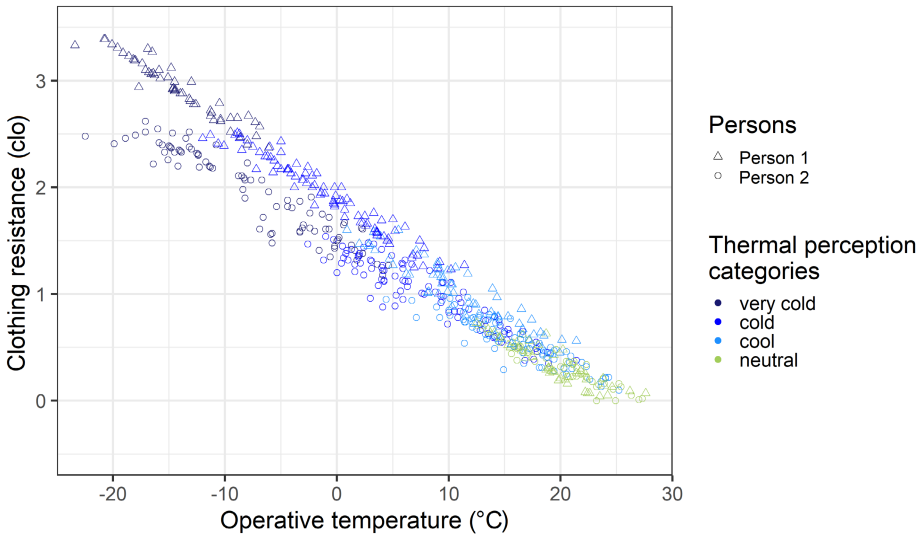

FIGURE 6 Scatter chart of clothing resistance of persons 1 and 2 as a function of operative temperature at actual average wind speed together with registered thermal sensation types (the average value of actual average wind speeds for persons 1 and 2 is 1.31 and 2.10 $m \cdot s^{-1}$, respectively) [Colour figure can be viewed at wileyonlinelibrary.com]

role of wind speed in shaping thermal load and thermal sensation is illustrated in Figure 5.

It can be seen that thermal sensation types are not denoted, despite the fact that the cooling effect of gust under strong thermal load may be significant. It is impossible to register this instantaneous thermal sensation effect with certainty; however, the thermal load-reducing effect can be estimated by model simulations comparing r_{cl}–T_o relationships obtained by average wind speed and gust. Based on the simulated results, the cooling effect of the gust results in an increase of r_{cl} values between 0 and 0.3 clo (the blue dots are above the red dots). This difference is somewhat smaller in the thermally neutral case, when r_{cl} is close to 0 clo.

As we said, the r_{cl}–T_o relationships vary from person to person. Differences between people are caused by differences between metabolic heat flux densities. The larger the M differences between people, the greater the corresponding r_{cl} differences. The r_{cl}–T_o scatter charts of persons 1 and 2 are presented in Figure 6.

Note that the M difference between persons 1 and 2 is small, it amounts to just 7 $W \cdot m^{-2}$, which is about 5% of their M values, and we can see that even this small difference is clearly noticeable. The greatest differences appear in extreme cold stress situations, they can be even 1 clo. The smallest differences are in thermally neutral cases, when they can reach values of 0.1–0.2 clo.

5.3 | Individual thermal sensation–thermal load relationships

The relationship between thermal perception obtained by persons 1 and 2 and thermal load represented by clothing resistance and operative temperature is illustrated in Figure 7a,b, respectively.

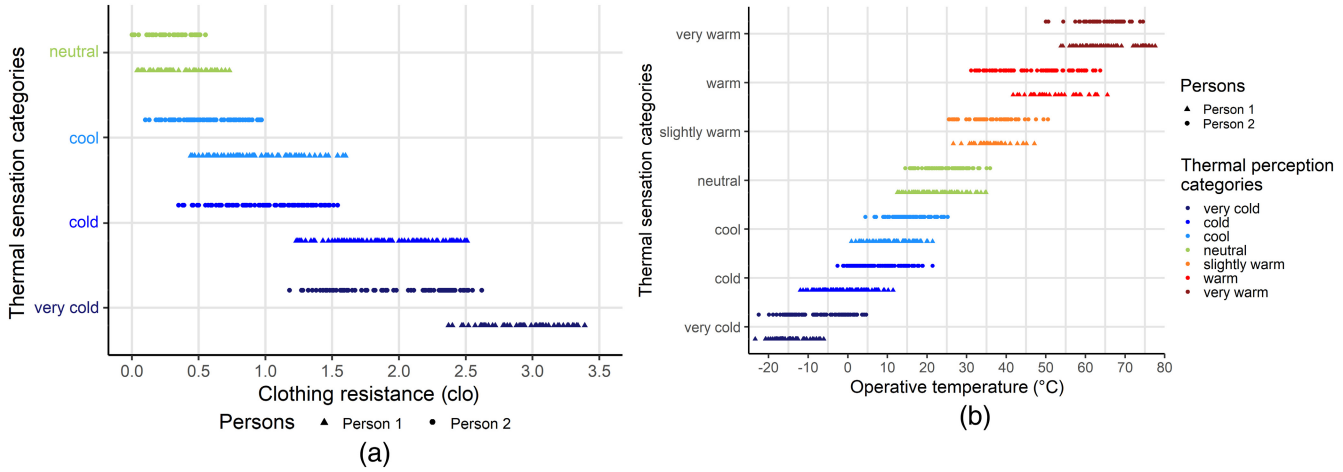

FIGURE 7 (a) Scatter chart of thermal perception obtained by persons 1 and 2 as function of clothing resistance for actual average wind speed values (the average value of actual average wind speeds for persons 1 and 2 is 1.31 and 2.1 $m \cdot s^{-1}$, respectively). (b) Scatter chart of thermal perception obtained by persons 1 and 2 as function of operative temperature for actual average wind speed values (in total 957 observations, the average value of actual average wind speed for persons 1 and 2 is 1.39 and 2.16 $m \cdot s^{-1}$, respectively) [Colour figure can be viewed at wileyonlinelibrary.com]

TABLE 3a Clothing resistance ranges of person 1 for different thermal sensation categories

Thermal sensation category	Clothing resistance (r_{cl}) range of person 1 (clo)
Neutral	$0 < r_{cl} \leq 0.4$
Neutral or cool	$0.4 < r_{cl} \leq 0.7$
Cool	$0.7 < r_{cl} \leq 1.2$
Cool or cold	$1.2 < r_{cl} \leq 1.6$
Cold	$1.6 < r_{cl} \leq 2.3$
Cold or very cold	$2.3 < r_{cl} \leq 2.5$
Very cold	$2.5 < r_{cl} \leq 3.5$

TABLE 3b Operative temperature ranges of person 1 for different thermal sensation categories

Thermal sensation category	Operative temperature (T_o) range of person 1 (°C)
Very warm	$65 \leq T_o < 80$
Very warm or warm	$54 \leq T_o < 65$
Warm	$47 \leq T_o < 54$
Warm or slightly warm	$41 \leq T_o < 47$
Slightly warm	$35 \leq T_o < 41$
Slightly warm or neutral	$26 \leq T_o < 35$
Neutral	$21 \leq T_o < 26$
Neutral or cool	$12 \leq T_o < 21$
Cool	$11 \leq T_o < 12$
Cool or cold	$1 \leq T_o < 11$
Cold	$-6 \leq T_o < 1$
Cold or very cold	$-12 \leq T_o < -6$
Very cold	$-25 \leq T_o < -12$

There are 957 points in total for persons 1 and 2, of which 138 points for the category "very cold," 200 points for "cold," 148 points for "cool," 174 points for "neutral," 87 points for "slightly warm," 110 points for "warm," and 100 points "very warm." Each point represents a weather situation. Based on Figure 7a,b, we also constructed Tables 3a and 3b for person 1, and Tables 4a and 4b for person 2, where the ranges of clothing resistance and operative temperature values and the associated thermal sensation categories are grouped and arranged in a continuous order.

Based on Figures 7 and Tables 3a, 3b, 4a, and 4b, we can see that (a) the r_{cl} difference between persons 1 and 2 is the smallest for the thermal perception category "neutral." As cold stress increases, r_{cl} differences between individuals also increase; in our case, these differences became the largest for the thermal perception category "very cold." (b) Discrete thermal perception categories are introduced for quantifying thermal sensation; however, it is obvious that the thermal sensation scale is continuous, which can be seen from the fact that the points in adjacent thermal sensation categories are mixed, that is there is no clear boundary between them. Of course, the mixing of points can be observed for both persons. This fact obviously shows that thermal perception is a subjective, individual-specific process.

TABLE 4a Clothing resistance ranges of person 2 for different thermal sensation categories

Thermal sensation category	Clothing resistance (r_{cl}) range of person 2 (clo)
Neutral	$0 < r_{cl} \leq 0.2$
Neutral or cool	$0.2 < r_{cl} \leq 0.3$
Neutral or cool or cold	$0.3 < r_{cl} \leq 0.6$
Cool or cold	$0.6 < r_{cl} \leq 1.0$
Cold	$1.0 < r_{cl} \leq 1.2$
Cold or very cold	$1.2 < r_{cl} \leq 1.6$
Very cold	$1.6 < r_{cl} \leq 3.0$

TABLE 4b Operative temperature ranges of person 2 for different thermal sensation categories

Thermal sensation category	Operative temperature (T_o) range of person 2 (°C)
Very warm	$64 \leq T_o < 80$
Very warm or warm	$49 \leq T_o < 64$
Warm or slightly warm	$36 \leq T_o < 49$
Warm or slightly warm or neutral	$30 \leq T_o < 36$
Slightly warm or neutral	$25 \leq T_o < 30$
Neutral or cool	$21 \leq T_o < 25$
Neutral or cool or cold	$15 \leq T_o < 21$
Cool or cold	$5 \leq T_o < 15$
Cold or very cold	$-4 \leq T_o < 5$
Very cold	$-25 \leq T_o \leq -4$

5.4 | Operative temperature–global radiation relationship

For a given region, the T_o–global radiation relationship is also an important human thermal climate characteristic. The scatter chart of T_o as function of global radiation for person 1 is presented in Figure 8.

Two ranges, a so-called "cold" (global irradiation is less than 200 W·m^{-2}) and a "warm" range (global irradiation is larger than 400 W·m^{-2}) can be distinguished. We can see that the scatter of the points is much larger in the "cold" than in the "warm" range. For $S = 0$, T_o can vary between −25 and +25°C, but for $S \geq 800$ W·m^{-2}, T_o varies between 59 and 79°C, that is, this range of T_o changes is much smaller than in the "cold" range. We can see that the upper limit of irradiation also clearly defines the upper limit of T_o.

5.5 | Operative temperature–air temperature relationship

From the point of view of human thermal load climatology, it is important to know the climatological relationship between T_o and T_a for a given region. T_a is easy to measure, while T_o contains the combined effect of T_a, radiation transfer and wind speed on thermal load. The scatter chart of T_o as function of T_a for persons 1 and 2 is presented in Figure 9.

Both point-clouds can be divided into two parts, a "cold" and a "warm" range. Those points lie in the "cold" range and are located between the thermal sensation categories "very cold" and "neutral." The points are coloured dark blue, blue, light blue, and green. In this range, T_o increases linearly with an increasing T_a. It can be seen that the rate of increase is person-dependent. The lowest T_o values in 2021 were around −20°C. But there have been also lower values in recent years (for instance, January 8, 2017). The lowest T_o values occur when the T_a values are very low and the sky is clear. This is usually in the morning in still air. In such cases, T_o may drop to around −35°C (T_a is around −25°C as on January 8, 2017), which can be considered as the lower limit of T_o in the climate of the Hungarian lowland.

The points in the "warm" range are located between thermal sensation categories "neutral" and "very warm." These are coloured green, orange, red, and dark red. In this range, T_a is roughly between 20 and 35°C, while T_o is between 20 and 80°C. As we see, the scatter of T_o is much greater than the scatter of T_a. The reason being that the scatter of T_o is determined by the combined scatter of T_a, solar irradiation and wind speed. The largest T_o values are around 80°C, when the solar irradiation is at its maximum and the wind speed is low. This is the upper limit of T_o in the climate of the Hungarian lowland.

The thermal load effect of cloudiness can be quantified by comparing the T_o–T_a difference for cloudy and clear sky conditions at night. Such a comparison is presented in Figure 10 for person 1.

T_a ranges from −10 to 30°C. In this T_a range, the T_o–T_a differences varied roughly between −2.5°C (cloudy sky) and −12.5°C (clear sky). When the sky is clear, the T_o–T_a differences seem to be smaller in absolute value (roughly between 8 and 10°C) for larger T_a values (T_a around 25°C), and conversely, the T_o–T_a differences seem to be larger in absolute value (roughly between 9 and 11°C), when T_a values are smaller (T_a around −5°C). In the case of a cloudy sky, the largest T_o–T_a differences are about −5°C and it can be observed for both lower (between 0 and 5°C) and higher (between 25 and 28°C) T_a values. In summary, the warming effect of cloudiness at night is very significant and it can be

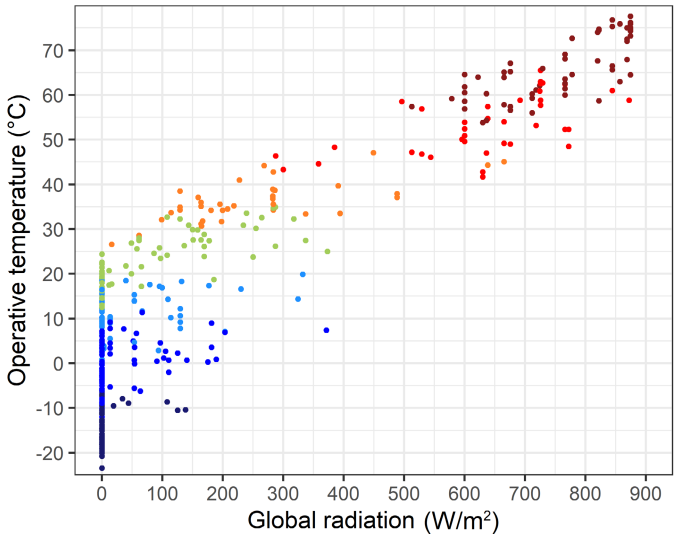

FIGURE 8 Scatter chart of operative temperature as function of global radiation together with thermal sensation types of person 1 for average wind speed values (the average value of actual average wind speed is 1.39 $m \cdot s^{-1}$) [Colour figure can be viewed at wileyonlinelibrary.com]

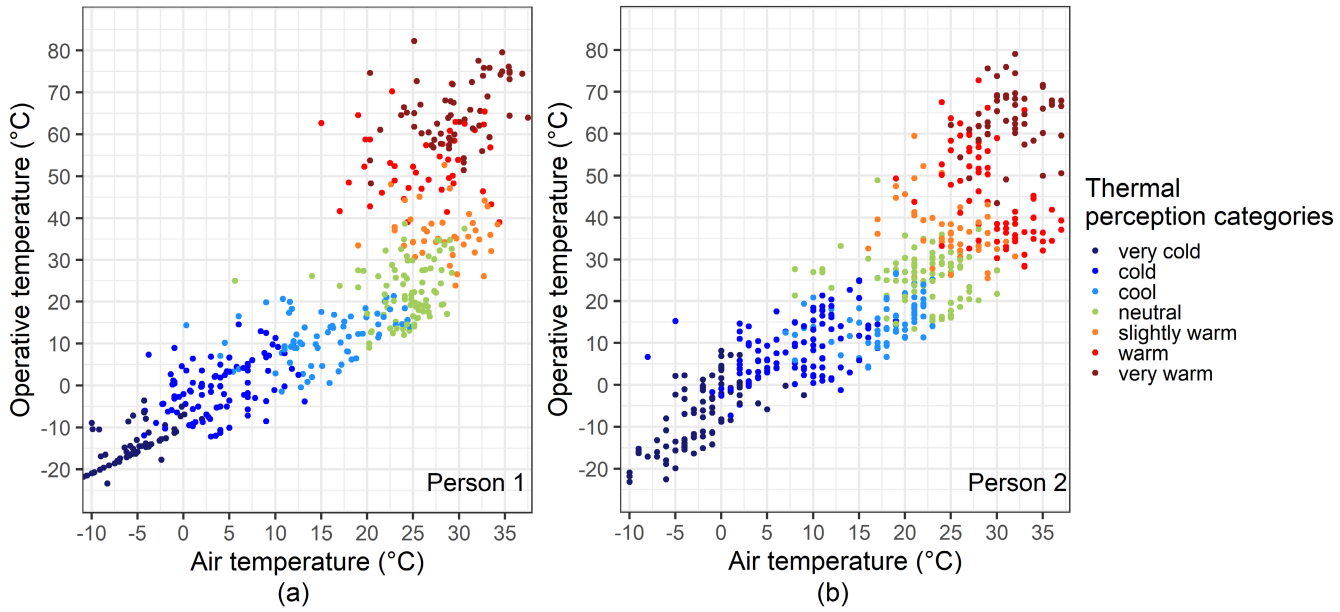

FIGURE 9 Scatter chart of operative temperature as function of air temperature together with thermal sensation types (a) for person 1 and (b) for person 2 for actual average wind speed values (the average value of actual average wind speed for person 1 and 2 is 1.39 and 2.16 $m \cdot s^{-1}$, respectively) [Colour figure can be viewed at wileyonlinelibrary.com]

higher than 10°C in the region of the Hungarian lowland.

5.6 | UTCI–clothing resistance and UTCI–operative temperature relationships

Phenomena can be better understood by comparing different models constructed for their description. Human thermal load and sensation can be equally simulated by the clothing resistance-operative temperature model and by the UTCI index model (Fiala *et al.*, 2011). A comparison of these two models is interesting for several reasons: (a) a simple model working in "backward mode" (clothing resistance is output variable) and a complex model working in "forward mode" (clothing resistance is input variable) are compared and, which is also important (b) such a model comparison does not yet exist (Blazejczyk *et al.*, 2012). In performing the comparison, the statistical version of the UTCI index model (Bröde *et al.*, 2012; the regression equation in Figure 8) is used, in which the air and mean radiation temperatures are the input variables. The UTCI–r_{cl} comparison is made for person 1. The scatter chart of UTCI as a function of clothing resistance for average wind speed and person 1 is presented in Figure 11.

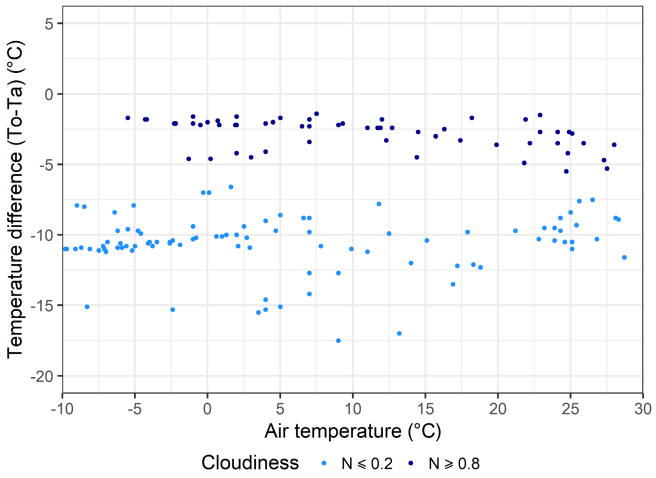

FIGURE 10 Scatter chart of T_o–T_a difference as function of T_a for cloudy (cloudiness between 0.8 and 1) and clear sky (cloudiness between 0 and 0.2) conditions at night for person 1 (the average value of actual average wind speed for cloudy and clear sky conditions is 1.30 and 1.59 m·s^{-1}, respectively) [Colour figure can be viewed at wileyonlinelibrary.com]

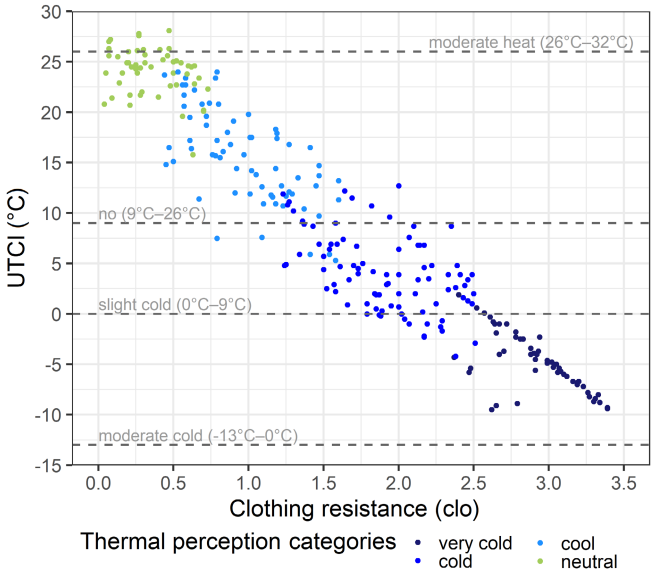

FIGURE 11 Scatter chart of UTCI as a function of clothing resistance for actual average wind speed and person 1 (the average value of actual average wind speed is 1.31 m·s^{-1}) [Colour figure can be viewed at wileyonlinelibrary.com]

Thermal stress categories related to UTCI index values and thermal perception categories related to r_{cl} are also depicted. The most striking fact is that in the UTCI comfort zone, the thermal perception categories "neutral," "cool," and "cold" occur; "cool" in the largest numbers practically throughout the entire zone, then "neutral" at the top of the zone, and finally the number of the "cold" cases is the smallest at the bottom of the zone. Note that "neutral" perceptions can be found mainly above UTCI = 20°C. It can be stated that in the UTCI comfort zone, the perception category "cool" is the most common for both persons. Note that there is no mixing of perception categories in the UTCI categories "slight cold" and "moderate cold." The UTCI–operative temperature scatter chart is also made for average wind speed and person 1. This is presented in Figure 12.

We can see that T_o varies between −24 and 0°C for −13°C ≤ UTCI ≤ 0°C (moderate cold stress, thermal perception "cool"), and similarly, it varies between 60 and 80°C for UTCI ≥ 46°C (extreme heat stress, thermal perception "very hot"). It can also be seen that the names of thermal perception categories are completely subjective.

As it is mentioned, the insulation value of clothing is a function of air temperature (Havenith *et al.*, 2012) in the UTCI model. In contrast, the insulation value of imagined clothing is estimated on the basis of thermal equilibrium between human body and environmental air in the r_{cl}-operative temperature model. Accordingly, these r_{cl} values are quite different. The scatter chart of the r_{cl} values obtained using the r_{cl}-operative temperature model and the UTCI-clothing model is presented in Figure 13.

It is obvious that the spread of the points decreases towards cold stress. In cold stress situations, r_{cl} values obtained by r_{cl}-operative temperature model are much higher than r_{cl} values obtained by UTCI-Fiala model. It is clear that people's clothing is determined not only by thermal balance but also by other mechanisms, so its accurate estimation is a difficult task.

5.7 | Clothing resistance–body composition parameter relationships

Since significant sexual dimorphism exists in the muscle and fat content of humans, and since human body structure changes significantly by age, the relationships between clothing resistance and body composition indices (fatBMI and muscleBMI) are investigated numerically by sex and age-group using human data from a Hungarian human data set (Zsákai and Bodzsár, 2016) and weather data for the winter situation presented in Table 1.

5.7.1 | Clothing resistance–fatBMI relationship

The scatter chart of the clothing resistance as a function of fatBMI by sex and age in an extreme winter weather situation is presented in Figure 14. Each point in Figure 14 represents one person.

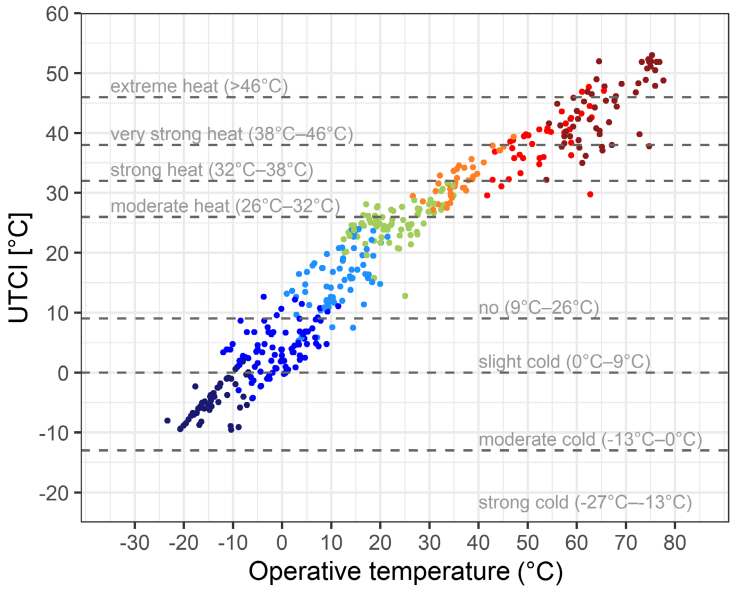

FIGURE 12 Scatter chart of UTCI as a function of operative temperature for actual average wind speed and person 1 (the average value of actual average wind speed is 1.39 $m \cdot s^{-1}$) [Colour figure can be viewed at wileyonlinelibrary.com]

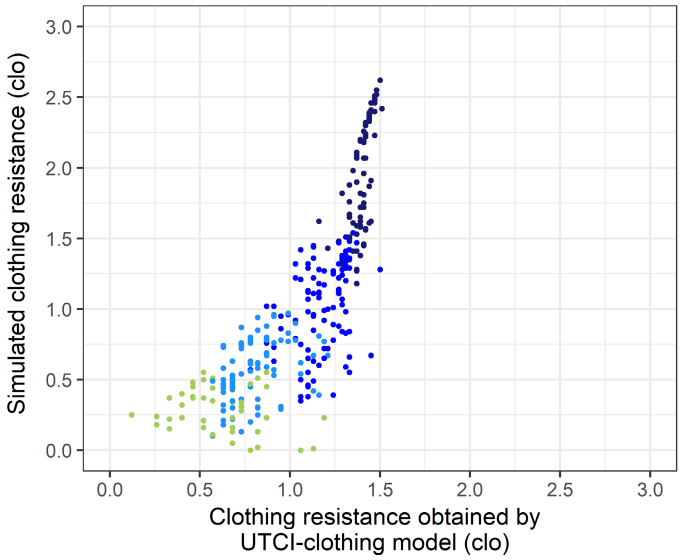

FIGURE 13 Scatter chart of clothing insulation values obtained by using r_{cl}-operative temperature model and UTCI-clothing model for actual average wind speed and person 2. Thermal perception categories are denoted by colours (the average value of actual average wind speed for person 2 is 2.10 $m \cdot s^{-1}$) [Colour figure can be viewed at wileyonlinelibrary.com]

In most cases, fatBMI varies between 1 and 15 $kg \cdot m^{-2}$. For the under-9 age group (boys and girls), fatBMI values are mostly between 1 and 7.5 $kg \cdot m^{-2}$; for the over-19 age group (men and women, the oldest person is 78 years), the fatBMI range is 1–15 $kg \cdot m^{-2}$, that is, with age, the fat content of the human body increases in most people. As we can see, there is an unequivocal correlation between clothing resistance and fatBMI regardless of sex and age. In all cases, the r_{cl} of females is somewhat larger than the r_{cl} of males since the M of females is slightly lower (about 10 $W \cdot m^{-2}$) than the M of males in most cases. Clothing resistance decreases slightly exponentially with an increase of fatBMI in both sexes going from the youngest to the oldest age group. In the youngest age group, the lowest r_{cl} values are around 1.7 clo and the associated fatBMI values are around 10 $kg \cdot m^{-2}$. In the oldest age group, the lowest r_{cl} values are around 1.5 clo, but in these cases, fatBMI values are greater than 15 $kg \cdot m^{-2}$. The clothing resistance difference between an obese adult male and an adult male having normal nutritional status (obese fatBMI is 10 $kg \cdot m^{-2}$, normal fatBMI is around 2 $kg \cdot m^{-2}$, if their height is around 170 cm, there is a cc. 30% difference in their body fat content) is about 0.5 clo. It is also obvious that there is a significant sexual dimorphism in the relationship between clothing resistance and fatBMI. The clothing resistance difference between a female and a male in the range of fatBMI of 2–10 $kg \cdot m^{-2}$ is about 0.1–0.3 clo in every subgroup. This relationship proves that metabolic heat flux density is also determined by fatBMI. However, the sexual dimorphism seems to be minimal for fatBMI above 10 $kg \cdot m^{-2}$.

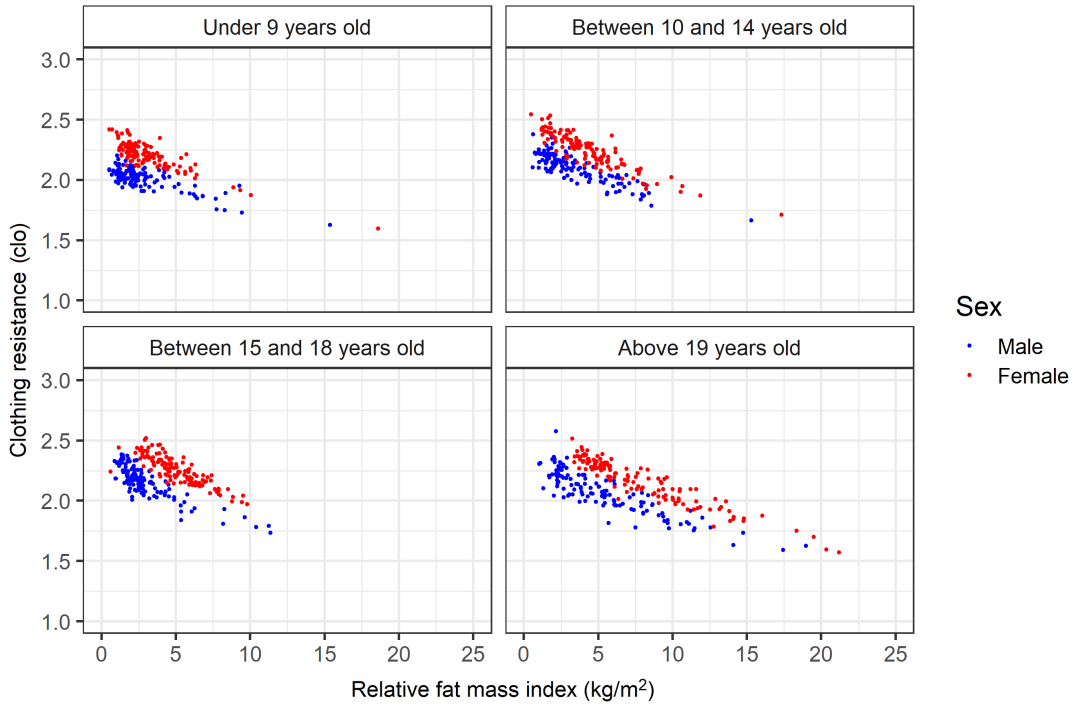

FIGURE 14 Clothing resistance as a function of relative fat mass index by sex and age in a winter weather situation [Colour figure can be viewed at wileyonlinelibrary.com]

5.7.2 | Clothing resistance–muscleBMI relationship

The relationship between clothing resistance and muscleBMI by sex and age in an extreme winter weather situation is presented in Figure 15.

The parameter muscleBMI ranges from 6 to 9 kg·m^{-2} for the youngest age group and from 7 to 15 kg·m^{-2} for the oldest age group, but there are only 4 points above 12 kg·m^{-2}. These scatter charts are very similar to the previous ones referring to fatBMI, that is, the nature of the dependence is the same, but differences can also be noticed, which are as follows: (a) although the r_{cl} differences between boy-girl or male–female are noticeable for the same muscleBMI values, they are smaller than for r_{cl}-fatBMI relationships. (b) The sexual dimorphism is more pronounced in the case of the youngest age-groups (age-groups between 7–9 and 10–14 years; Figure 15). Clothing resistance for girls is 0.2–0.3 clo higher than for boys. (c) From the age of 15, the muscularity of males and females is getting more and more distinct; therefore, there is no point in comparing the clothing resistance for a male and a female having the same muscleBMI.

6 | DISCUSSION

Human modelling is the central issue in the science of human thermal load and perception modelling. There are two opposing approaches: one uses a "standardized" human, the other uses individuals. In scientific practice, the former approach is widespread (e.g., Höppe, 1999; Blazejczyk *et al.*, 2013). It was not until recently that methods using the latter approach appeared (e.g., Thuomaala *et al.*, 2013; Zhou *et al.*, 2013; Schweiker *et al.*, 2018; Ács *et al.*, 2021b). In both approaches, human modelling involves modelling of (a) clothing, (b) metabolic heat flux density related to the activity, and (c) human thermal perception. As we know, (a) clothing can be extremely individual and it can be culturally determined, (b) the interpersonal variability of M increases with increasing intensity of activity (Campbell and Norman, 1998), and (c) the simulation of human thermal perception is an extremely complex task due to the physiological nature of thermoregulatory processes. In our method, we intended to address these issues as simply as possible taking into account people's individual characteristics. Based on these principles (simplicity and individualization), the clothing resistance parameter as an input variable in simulating thermal load has been eliminated, the walking person's M is parameterized in the simplest possible way, and finally thermal perception is not simulated but observed. The resulting model is an inverse Fanger model, because clothing resistance is not an input but an output variable. The thermal insulation value of an imaginary attire is simulated, which creates a thermal balance between the human body and its environment. The thermal resistance

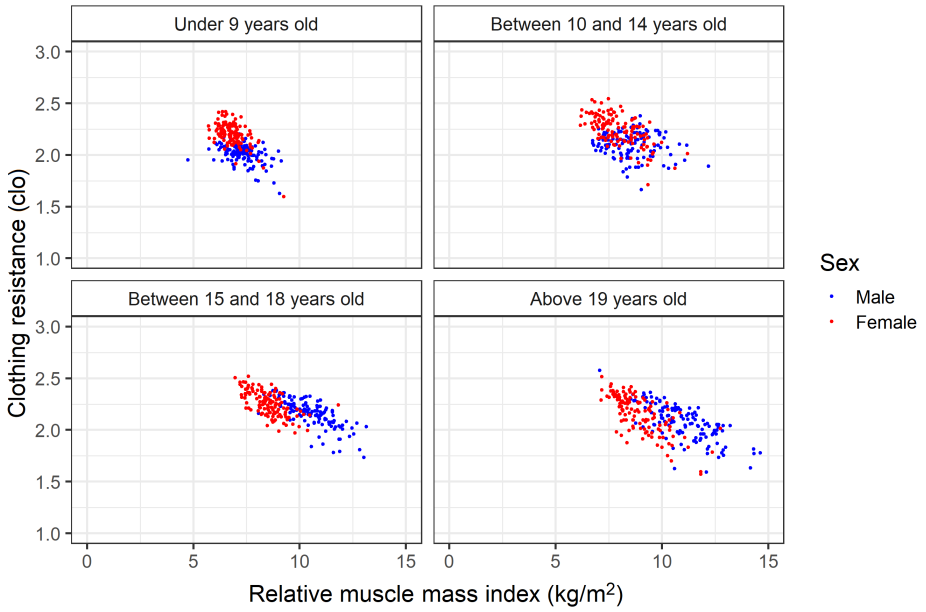

FIGURE 15 Clothing resistance as a function of relative muscle mass index by sex and age in a winter weather situation [Colour figure can be viewed at wileyonlinelibrary.com]

of this imaginary clothing should not be confused with the thermal resistance of real, worn clothing.

The behaviour of the model is also analysed by comparing its results with results obtained from the UTCI-model. In comparison, its statistical version (Bröde *et al.*, 2012) is used. This is chosen because the UTCI-clothing model is extremely simple, it uses only air temperature as input (Havenith *et al.*, 2012). The clothing resistance values obtained from the UTCI model and the r_{cl}-operative temperature model are compared in Figure 13. As we see, the obtained values differ markedly, but this is expected since one refers to real, worn clothing and the other to imaginary clothing. The agreement of thermal sensation results is acceptable. Note that according to the r_{cl}-operative temperature model the UTCI-model comfortable zone seems to be a little bit broad because in it the r_{cl}-operative temperature model thermal sensation types "neutral," "cool," and "cold" are registered. It should be noted that of these three thermal sensation types, "cool" was the most common. Thermal perception observation is performed by people (persons 1 and 2) with a BMI around 25 kg·m^{-2}, this value is very close to the median value of the BMI for the Hungarian database. It should also be noted that the fatBMI and muscleBMI values of the observers (see Figures 14 and 15, person 1: fatBMI = 4.07 kg·m^{-2}, muscleBMI = 11.7 kg·m^{-2}, person 2: fatBMI = 10.9 kg·m^{-2}, muscleBMI = 9.68 kg·m^{-2}) are not located at the edges of the point cloud of the database.

The effect of interpersonal variations on thermal load and thermal sensation is well-known. This is investigated in many studies (e.g., Kántor *et al.*, 2012) and is also illustrated in this study. The interpersonal variation effect is the smallest in the thermal sensation category "neutral" and decreases with the decrease of human activity (Ács *et al.*, 2022). It is practically negligible for people who are in a supine position and in thermal equilibrium with the environment.

The process of thermal perception cannot be simulated without thermal perception observations. Human thermal climate characteristics can only be determined on the basis of long-term observations of individuals. No human thermal climate has been characterized to date based on individual, long-term concurrent observations of weather and thermal perception. This can be explained by the fact that models based on the concept of the "standardized human" had become widespread in scientific practice. Based on long-term individual observations, the following main human thermal climate characteristics for the Hungarian lowland can be highlighted:

1. T_o can vary between −20 and 80°C, similarly r_{cl} variations for person 1 are between 3.5 and 0 clo. These values of T_o represent the annual minimum and maximum values in 2021. The T_o temperature of about 80°C can be considered as the upper limit of the thermal load in the Hungarian lowland, as it was recorded in June (June 24) between noon and 1 p.m., when solar radiation was strongest during the year, at an air temperature of 34.7°C. At such a thermal load, the thermal sensation is "unbearably warm" rather than "very warm." We also know that the lower limit of thermal load in the Hungarian lowland is between −30 and −40°C and it depends on air temperature and it can only be met when the sky is clear. Note that we cannot obtain information on such extreme thermal loads if we are using climatic data (Ács *et al.*, 2021a).

Of course, there are studies focusing on extreme bioclimatic conditions in lowland regions of the Carpathian Basin, nevertheless, other methodology and aspects are used, so, any comparison is cumbersome. Such a study is, for instance, the work of Bašarin *et al.* (2018).

2. In the case of large thermal load, the differences between individual thermal loads are also large. In such cases, significant differences in thermal perception can appear since thermal perception depends not only on M but also on other human factors, such as body fitness. This is, for instance, demonstrated in the work of Thuomaala *et al.* (2013). Our results related to r_{cl}–fatBMI and r_{cl}–muscleBMI relationships agree with Thuomaala *et al.*'s (2013) results, but note that our results are related to the thermal load, while Thuomaala *et al.*'s (2013) results are related to thermal perception. They used a very complex human thermal model capable of simulating thermal perception. In the cases of extreme thermal load, our results also suggest that there is a significant sexual dimorphism in the relationship between r_{cl} and fatBMI. This is caused by the significant differences in body fat content of men and women (Jackson *et al.*, 2002). It should also be mentioned that both body composition parameters change dynamically throughout a human lifetime. fatBMI grows in the first 1–2 years, then decreases until puberty and then grows again until people die. Muscle mass increases strongly until the age of 20–25 and then stagnates for a period of time, after which it begins to decline until death, even reaching the values typical for childhood (Bodzsár, 2000; Zsákai *et al.*, 2016). These biological changes also modify the thermal load, especially in extreme situations such as that discussed above. We have to see that thermal load is also biologically determined, which changes dynamically in a person's lifetime, to an extent that is not negligible. It should be noted that these effects cannot be simulated by using models based on the concept of a "standard human."
3. The interpersonal variation effect of r_{cl} is the smallest in the "neutral" thermal sensation category. In this case, T_o varies roughly between 20 and 30°C in the Hungarian lowland and for people acclimated to its climate. This agrees with results of Ács *et al.* (2021a). Note that thermal indices created for "standard human" must also be calibrated if climates differ from the climate for which the scale of thermal sensation categories has been established (Krüger *et al.*, 2021).
4. We also have human thermal climate information for the nighttime period of the day. In this period of day, r_{cl} can vary between 0 and 3.5 clo, the corresponding T_o variations are between 25 and −23°C. As we can see, the annual fluctuation of T_o in the nighttime period of day is around 50°C. These variations of T_o are caused mostly by variations of air temperature and cloudiness since the wind speed values are low in the vast majority of cases. The thermal sensation types "very cold," "cold," "cool," and "neutral" characterized the period. Note that the combined effect of air temperature, cloudiness and wind speed never resulted in the thermal sensation type "slightly warm." We dare to say this, because we literally conducted a hunt for such cases. But there may be such cases in built-up parts of cities.
5. The performance of the model is examined by selecting and comparing results obtained in different conditions. The effect of solar radiation on thermal load is analysed by comparing T_o and global radiation. Similarly, the effect of cloudiness by comparing T_o–T_a differences in the nighttime period, when the sky is clear and completely overcast, and finally, the effect of wind speed by comparing r_{cl} values for average wind speed and gust. The results obtained suggest that the model is working well and its behaviour is consistent with those sensitivity test results obtained by models using the concept of "standard human" (e.g., Höppe, 1999; Kim *et al.*, 2009; Bröde *et al.*, 2012).

6.1 | Limitations of the study

As a matter of fact, it can be seen that biological variance is poor (just two observers who are part of the outdoor environment), this shortcoming is offset by the much greater environmental variability. In our case, the human–climate relationship is direct, consequently as strong as possible because (a) the human is a person, not a "standardized human" and (b) the environment is climate, that is, the long-term time series of weather events, and not the "standard environment." The human–climate relationship is analysed, not the climate itself since the observer is part of the outdoor environment. Climate is reflected in humans by the magnitude of thermal load and the type of thermal perception, which are the relationship characteristics of the person-climate system. By definition, these features are relative. The long-term time series of thermal load values and thermal perception types are like a network; the observers can be considered as the nodes of this network. At the moment, there are only few nodes (e.g., Kelemen, 2020), the density of the network, of course, increases with the number of nodes. In summary: by determining human thermal loads and thermal perception types, it is not the climate, but the human–climate relationship, which is being characterized. From this point of view, even having a network

with only one node makes sense. By the way, the climate must always be viewed in such a relational interpretation (Rovelli, 2022).

7 | CONCLUSION

In this research, individual, local, and long-term observations of weather and human thermal perception have been carried out to obtain more information on human–climate relationship in the Hungarian lowland. A clothing resistance-operative temperature model was used to study the characteristics of human thermal load and perception. The behaviour of the model is investigated not only with respect to the changes of weather elements but also with respect to the changes of body composition parameters.

From our research, the following conclusions can be drawn. (a) Each human–climate relationship can be characterized by an upper (absolute maximum) and a lower (absolute minimum) human thermal load limit. These values can be estimated by using both observations and numerical simulations. (b) In the climate of the Hungarian lowland, human thermal load is mostly determined by the combined effect of air temperature and radiation. Extreme warm and cold operative temperatures cannot occur without the presence of strong solar irradiation and clear sky conditions, respectively. (c) The interpersonal variability of human thermal load increases with increasing heat lack. It is the largest in "very cold" thermal perception category; it is the lowest in the "neutral" thermal perception category. (d) Regarding the relationship between human thermal load and human factors, the role of fatBMI in formation of individual human thermal load should be highlighted. In cold stress situations, the interpersonal variability of fatBMI considerably determines the interpersonal variability of clothing resistance. Significant sexual dimorphism can also be observed in the range of fatBMI of 2–10 $kg \cdot m^{-2}$. Finally, (e) human thermal load changes dynamically over a person's lifetime, because of the dynamic change of body mass and body composition parameters.

ORCID

Ferenc Ács https://orcid.org/0000-0002-1611-6839

REFERENCES

Ács, F., Kristóf, E. and Zsákai, A. (2019) New clothing resistance scheme for estimating outdoor environmental thermal load. *Geographica Pannonica*, 23(4), 245–255.

Ács, F., Zsákai, A., Kristóf, E., Szabó, A.I. and Breuer, H. (2021a) Human thermal climate of the Carpathian Basin. *International Journal of Climatology*, 41(S1), E1846–E1859. https://doi.org/10.1002/joc.6816.

Ács, F., Zsákai, A., Kristóf, E., Szabó, A.I., Feddema, J. and Breuer, H. (2021b) Clothing resistance and potential evapotranspiration as thermal climate indicators—the example of the Carpathian region. *International Journal of Climatology*, 41(5), 3107–3120. https://doi.org/10.1002/joc.7008.

Ács, F., Zsákai, A., Kristóf, E. and Szalkai, Z. (2022) What is the most appropriate person for human thermal climate studies to be used for climate classification puposes. In: Dunkel (Ed.) *Proceeding of the 5th Conference of Medical Meteorology, Hungarian Meteorological Society*. Budapest: Hungarian Meteorological Society. pp. 13–18 ISBN 978-963-8481-15-3.

Auliciems, A. and Kalma, J.D. (1979) A climatic classification of human thermal stress in Australia. *Journal of Applied Meteorology*, 18, 616–626. https://doi.org/10.1111/j.14678470.1981.tb00373.x.

Bašarin, B., Lukić, T., Mesaros, M., Pavić, D., Djordjević, J. and Matzarakis, A. (2018) Spatial and temporal analysis of extreme bioclimate conditions in Vojvodina, Nothern Serbia. *International Journal of Climatology*, 38(1), 142–157.

Blazejczyk, K., Bröde, P., Fiala, D., Havenith, G., Holmér, I., Jendritzky, G., Kampmann, B. and Kunert, A. (2010) Principles of the new Universal Thermal Climate Index (UTCI) and its application to bioclimatic research in European scale. *Miscellanea Geographica*, 14, 91–102.

Blazejczyk, K., Epstein, Y., Jendritzky, G., Staiger, H. and Tinz, B. (2012) Comparison of UTCI to selected thermal indices. *International Journal of Biometeorology*, 56, 515–535. https://doi.org/10.1007/s00484-011-0453-2.

Blazejczyk, K., Jendritzky, G., Bröde, P., Fiala, D., Havenith, G., Epstein, Y., Psikuta, A. and Kampmann, B. (2013) An introduction to the universal thermal climate index (UTCI). *Geographia Polonica*, 86(1), 5–10.

Blazejczyk, K. and Krawczyk, B. (1994) Bioclimatic research of the human heat balance. *Polish Academy of Sciences, Institute of Geography and Spatial Organization*, 28, 70.

Bodzsár, É.B. (2000) A review of Hungarian studies on growth and physique of children. *Acta Biologica Szegediensis*, 44(1–4), 139–153.

Bröde, P., Fiala, D., Blazejczyk, K., Holmér, I., Jendritzky, G., Kampmann, B., Tinz, B. and Havenith, G. (2012) Deriving the operational procedure for the universal thermal climate index (UTCI). *International Journal of Biometeorology*, 56(3), 481–494.

Campbell, G.S. and Norman, J.M. (1998) *An Introduction to Environmental Biophysics*, Second edition. New York: Springer. 286 pp., ISBN-0-387-94937-2.

Dubois, D. and Dubois, E.F. (1915) The measurement of the surface area of man. *Archives of Internal Medicine*, 15, 868–881. https://doi.org/10.1001/archinte.1915.00070240077005.

Enescu, D. (2019) Models and indicators to assess thermal sensation under steady-state and transient conditions. *Energies*, 12(5), 841. https://doi.org/10.3390/en12050841.

Fanger, P.O. (1970) *Thermal Comfort: Analysis and Applications in Environmental Engineering*. PhD Thesis, Danmarks tekniske højskole. Copenhagen: Danish Technical Press. 244 pp., ISBN: 8757103410 9788757103410.

Fanger, P.O. (1973) Assessment of man's thermal comfort in practice. *British Journal of Industrial Medicine*, 30, 313–324.

Feddema, J.J. (2005) A revised Thornthwaite-type global climate classification. *Physical Geography*, 26, 442–466.

Fehér, P., Annár, D., Zsákai, A. and Bodzsár, É. (2019) Pszichoszomatikus tünetek gyakoriságát befolyásoló tényezők 18–90 éves nők körében. *Anthropológiai Közlemények*, 60, 65–77. https://doi.org/10.20330/AnthropKoz.2019.60.65.

Fiala, D. (1998) *Dynamic Simulation of Human Heat Transfer and Thermal Comfort*. PhD Thesis. Leicester: De Monfort University Leicester and Fh Stuttgart – Hochschule für Technik 293 pp.

Fiala, D., Havenith, G., Bröde, P., Kampmann, B. and Jendritzky, G. (2011) UTCI-Fiala multi-node model of human heat transfer and temperature regulation. *International Journal of Biometeorology*, 56(3), 1–13.

Finn, K.J., Saint-Maurice, P.F., Karsai, I., Ihász, F. and Csányi, T. (2015) Agreement between Omron 306 and biospace InBody 720 bioelectrical impedance analyzers (BIA) in children and adolescents. *Research Quaterly for Exercise and Sport*, 86(Suppl. 1), S58–S65. https://doi.org/10.1080/02701367.2015.1042998.

Gagge, A.P., Stolwijk, J.A.J. and Nishi, Y. (1971) An effective temperature scale based on a simple model of human physiological regulatory response. *ASHRAE Transactions*, 77, 247–257.

Gilligan, I. (2010) The prehistoric development of clothing: archaeological implications of a thermal model. *Journal of Archaeological Method and Theory*, 17(1), 15–80. https://doi.org/10.1007/s10816-009-9076-x.

Gulyás, Á. and Matzarakis, A. (2009) Seasonal and spatial distribution of physiologically equivalent temperature (PET) index in Hungary. *Időjárás*, 113(3), 221–231.

Havenith, G., Fiala, D., Blazejczyk, K., Richards, M., Bröde, P., Holmér, I., Rintamaki, H., Benshabat, Y. and Jendritzky, G. (2012) The UTCI-clothing model. *International Journal of Biometeorology*, 56(3), 461–470.

Höppe, P. (1984) Die Energiebilanz des Menschen. In: *Wissenschaftlichen Mitteilungen*. München: Meteorologisches Institut München. Nr 49.

Höppe, P. (1993) Heat balance modelling. *Experientia*, 49, 741–746.

Höppe, P. (1999) The physiological equivalent temperature – a universal index for the biometeorological assessment of the environment. *International Journal of Biometeorology*, 43, 71–75.

Innova Air Tech Instruments (2002) Thermal Comfort, *Innova Air Tech Instruments*, 32 pp. (it is available from the authors on the request).

Jackson, A.S., Stanforth, P.R., Gagnon, J., Rankinen, T., Leon, A.S., Rao, D.C., Skinner, J.S., Bouchard, C. and Wilmore, J.H. (2002) The effect of sex, age and race on estimating percentage body fat from body mass index: the Heritage Family Study. *International Journal of Obesity*, 26, 789–796.

Kántor, N., Égerházi, L. and Unger, J. (2012) Subjective estimation of thermal environment in recreational urban spaces—part 1: investigations in Szeged, Hungary. *International Journal of Biometeorology*, 56, 1089–1101.

Kelemen, B. (2020) *Weather Variability from the Point of View of Human Thermal Load and Thermal Sensation*. MSc Thesis. Budapest: ELTE, Department of Meteorology 63 pp. (in Hungarian).

Kim, J., Kim, K.R., Choi, B.-C., Lee, D.-G. and Kim, J.-S. (2009) Regional distribution of perceived temperatures estimated by the human heat budget model (the Klima-Michel model) in South-Korea. *Advances in Atmospheric Sciences*, 26(2), 275–282.

Köppen, W. (1936) The geographic system of climates (original: das geographische system der Klimate). In: Köppen, W. and Geiger, R. (Eds.) *Handbuch der Klimatologie*, Vol. 1, Teil C. Berlin: Borntraeger. 44 pp.

Krüger, E.L., Vieira Silva, T.J., Silveira Hirashima, S.Q., Cunha, E. G. and Rosa, L.A. (2021) Calibrating UTCI'S comfort assessment scale for three Brazilian cities with different climatic conditions. *International Journal of Biometeorology*, 65, 1463–1472.

Matzarakis, A. and Mayer, H. (1996) Human-biometeorologische Untersuchungen in den höheren Lagen des Schwarzwaldes. In: *Proceedings of the 24th international conference on alpine meteorology*. Ljubljana. pp. 417–423.

Matzarakis, A. and Mayer, H. (1997) Heat stress in Greece. *International Journal of Biometeorology*, 41, 34–39.

Matzarakis, A., Mayer, H. and Iziomon, M.G. (1999) Applications of a universal thermal index: physiological equivalent index. *International Journal of Biometeorology*, 43, 76–84.

Matzarakis, A., Rutz, F. and Mayer, H. (2007) Modelling radiation fluxes in simple and complex environments – application of the RayMan model. *International Journal of Biometeorology*, 51, 323–334.

Mayer, H. and Höppe, P. (1987) Thermal comfort of man in different urban environments. *Theoretical and Applied Climatology*, 38, 43–49.

McNall, P.E., Jaax, J., Rohles, F.H., Nevins, R.G. and Springer, W. (1967) Thermal comfort (thermally neutral) conditions for three levels of activity. *ASHRAE Transaction*, 73(1), 1.3.1–1.3.14.

Mifflin, M.D., St Jeor, S.T., Hill, L.A., Scott, B.J., Daugherty, S.A. and Koh, Y.O. (1990) A new predictive equation for resting energy expenditure in healthy individuals. *The American Journal of Clinical Nutrition*, 51, 241–247. https://doi.org/10.1093/ajcn/51.2.241.

Mihailović, D.T. and Ács, F. (1985) Calculation of daily amounts of global radiation in Novi Sad. *Időjárás*, 89, 257–261 (in Hungarian).

Milošević, D.D., Savić, S.M., Marković, V., Arsenović, D. and Šećerov, I. (2016) Outdoor human thermal comfort in local climate zones of Novi Sad (Serbia) during heat wave period. *Hungarian Geographical Bulletin*, 65, 129–137.

Mohan, M., Gupta, A. and Bhati, S. (2014) A modified approach to analyse thermal comfort classification. *Atmospheric and Climate Sciences*, 4, 7–19.

Nevins, R.G., Rohles, F.H., Springer, W. and Feyerherm, A.M. (1966) Temperature-humidity chart for thermal comfort of seated persons. *ASHRAE Transactions*, 72, 283–291.

Ogulata, R.T. (2007) The effect of thermal insulation of clothing on human thermal comfort. *Fibres and Textiles in Eastern Europe*, 15(2), 67–72.

Pecelj, M., Matzarakis, A., Vujadinović, M., Radovanović, M., Vagić, N., Đurić, D. and Cvetković, M. (2021) Temporal analysis of urban-suburban PET, mPET and UTCI indices in Belgrade (Serbia). *Atmosphere*, 12(7), 916. https://doi.org/10.3390/atmos12070916.

Potchter, O., Cohen, P., Lin, T.P. and Matzarakis, A. (2018) Outdoor human thermal perception in various climates: a comprehensive review of approaches, methods and quantification. *Science of The Total Environment*, 631–632, 39–406. https://doi.org/10.1016/j.scitotenv.2018.02.276.

Rohles, F.H. (1970) *Thermal Sensation of Sedentary Man in Moderate Temperatures*. Special report of Institute for Environmental Research. Manhattan: Kansas State University.

Rovelli, C. (2022) *Helgoland: Making Sense of the Quantum Revolution*. Budapest: Park Kiadó 269 pp., ISBN 978-963-355-725-9 (in Hungarian).

Salma, I., Vörösmarty, M., Gyöngyösi, A.Z., Thén, W. and Weidinger, T. (2020) What can we learn about urban air quality with regard to the first outbreak of the COVID-19 pandemic? A case study from the Central Europe. *Atmospheric Chemistry and Physics*, 20, 15725–15742. https://doi.org/10.5194/acp-20-15725-2020.

Schweiker, M., Huebner, G.M., Kingma, B.R.M., Kramer, M. and Pallubinsky, H. (2018) Drivers of diversity in human thermal perception – a review for holistic comfort models. *Temperature*, 5(4), 308–342. https://doi.org/10.1080/23328940.2018.1534490.

Staiger, H., Laschewski, G. and Matzarakis, A. (2019) Selection of appropriate thermal indices for applications in human biometeorological studies. *Atmosphere*, 10(1), 18. https://doi.org/10.3390/atmos10010018.

Thuomaala, P., Holopainen, R., Piira, K. and Airaksinen, M. (2013) Impact of individual characteristics – such as age, gender, BMI and fitness – on human thermal sensation. In: *Proceedings of BS2013: 13th conference of international building performance simulation association*. Chambery. pp. 2305–2310.

Unger, J., Skarbit, N., Kovács, A. and Gál, T. (2020) Comparison of regional and urban outdoor thermal stress conditions in heatwave and normal summer periods: a case study. *Urban Climate*, 32, 100619.

Utczás, K., Zsákai, A., Muzsnai, Á., Fehér, V.P. and Bodzsár, É. (2015) Radiológiai és ultrahangos módszerrel végzett csontélet-kor-becslések összehasonlító elemzése 7–17 éveseknél (the analysis of bone age estimations performed by radiological and ultrasonic methods in children aged between 7–17 year). *Anthropológiai Közlemények*, 56, 129–138 (in Hungarian).

Weyand, P.G., Smith, B.R., Puyau, M.R. and Butte, N.F. (2010) The mass-specific energy cost of human walking is set by stature. *Journal of Experimental Biology*, 213, 3972–3979. https://doi.org/10.1242/jeb.048199.

Zhou, X., Lian, Z. and Lan, L. (2013) An individualized human thermoregulation model for Chinese adults. *Building and Environment*, 70, 257–265.

Zsákai, A. and Bodzsár, É. (2016) A reprodukciós öregedés és csontszerkezet változásának kapcsolata nőknél. *Anthropológiai Közlemények*, 57, 77–84. https://doi.org/10.20330/AnthropKozl.2016.57.77.

Zsákai, A., Karkus, Z., Utcás, K., Biri, B., Sievert, L. and Bodzsár, É.B. (2016) Body fatness and endogenous sex hormones in the menopausal transition. *Maturitas*, 87, 18–26.

How to cite this article: Ács, F., Kristóf, E., & Zsákai, A. (2023). Individual local human thermal climates in the Hungarian lowland: Estimations by a simple clothing resistance-operative temperature model. *International Journal of Climatology*, *43*(3), 1273–1292. https://doi.org/10.1002/joc.7910